ACS APPLIED BIO MATERIALS

www.acsabm.org

Article

Highly Sensitive Protein Detection by Asymmetric Mach–Zehnder Interferometry for Biosensing Applications

Melissa J. Goodwin, Geert A. J. Besselink, Floris Falke, Arnoud S. Everhardt, Jeroen J. L. M. Cornelissen, and Jurriaan Huskens*

Cite This: *ACS Appl. Bio Mater.* 2020, 3, 4566–4572

Read Online

ACCESS | Metrics & More | Article Recommendations

ABSTRACT: The sensitivity and performance of an asymmetric Mach–Zehnder interferometer (aMZI) were compared to those of quartz crystal microbalance with dissipation (QCM-D). The binding of streptavidin to sensor chips coated with poly-L-lysine (PLL), modified with biotin and oligoethyleneglycol (OEG) (PLL-biotin), was used to compare the binding signals obtained from both technologies. PLL-biotin proved to be an efficient method to add bioreceptors to both the QCM-D and aMZI chips. The final, saturated value of streptavidin binding was compared with those from aMZI (253 ng cm^{-2}) and QCM-D (460 ng cm^{-2}). These values were then used to evaluate that 45% of the measured streptavidin mass in the QCM-D came from hydrodynamically coupled water. Importantly, the signal-to-noise ratio of the aMZI was found to be 200 times higher than that of the QCM-D. These results indicate the potential of the aMZI platform for highly sensitive and accurate biosensing applications.

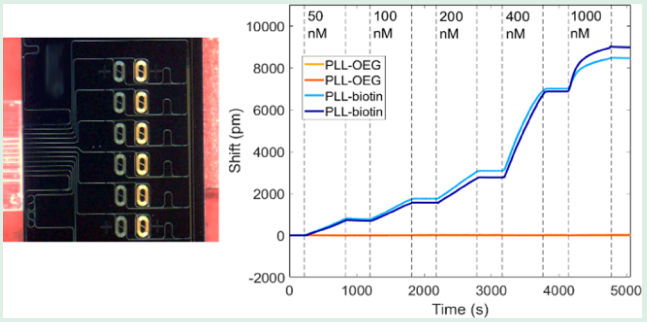

KEYWORDS: *biosensing, asymmetric Mach–Zehnder interferometry, quartz crystal microbalance, surface plasmon resonance, poly-l-lysine*

INTRODUCTION

Biosensors[1−3] have seen a great increase of interest in the last years, where they encompass devices as common as blood glucose sensors for helping the maintenance of blood sugar for diabetics,[4] to as specialistic as the detection of biomarkers for specific cancers.[5,6] Such biosensors are hereby used to detect (bio)chemical compounds mediated by isolated enzymes, immunosystems, tissues, organelles, or whole cells utilizing, for example, electrochemical[7−11] and optical devices.[12−14]

Optical biosensors have several key advantages over other methods. As they are significantly less affected by electromagnetic interference, they can be self-referencing, contain an antifouling reference on the same chip as the detector, and they can also be integrated with common optical methods like Raman scattering, which makes use of the unique fingerprint of an analyte to perform in situ spectroscopy.[15] A biosensor needs both specificities for the desired analyte, even in a complex matrix such as blood, and high sensitivity to the analyte to detect the markers in concentrations that can be as low as femtogram per milliliter.[16] Up to now, electrochemical sensors have been able to reach sensitivities that optics could not rival.[17] However, recent advances in the field of optics and integrated optics have greatly reduced the limit of detection of optical biosensors down to biologically relevant values.[18,19]

One such optical technique is the asymmetric Mach–Zehnder interferometer (aMZI), which detects changes in the refractive index.[20,21] The aMZI devices used in this study were fabricated using TriPleX technology.[22] The fabricated chips consist of stoichiometric Si_3N_4 waveguides with SiO_2 cladding, which forms a photonic integrated circuit (PIC). The SiO_2 cladding is locally removed to form the so-called sensing window, which allows the analyte to make contact with the waveguide. In the aMZI design, the waveguide splits the incoming light into two arms, one of which is exposed to the analyte and the other is never exposed to the analyte and used as a reference. This asymmetry is introduced deliberately in the interferometer to allow an interference pattern to be detected on the recombination of the two aMZI arms. When the analyte solution interacts with the evanescent field of the waveguide in the sensing window, changes in the refractive index result in a phase shift of the laser wavelength (in picometer, pm) in the interference pattern. The aMZI is sensitive both to changes in the refractive index of the liquid (the bulk shift) and the binding of the targeted specific analyte to the surface.[18,23] Initial proof-of-concept experiments have been performed

Received: April 29, 2020
Accepted: June 12, 2020
Published: June 12, 2020

using these aMZI devices as biosensors,[20,24−29] but it is important to perform a direct comparison of this technique to the current standard technology to verify its efficacy.

To provide a proof of concept of using the aMZI as a biosensor, it is necessary to have a method of reliably attaching bioreceptors to the substrate to achieve selectivity and specificity. One such method is the use of poly-L-lysine (PLL). PLL provides a versatile and robust method of attaching (bio)probes to a wide range of different substrates.[30,31] The charged amine groups of the lysine moieties enable PLL to strongly adsorb to any negatively charged surface, such as any surface that can be treated with UV/ozone, oxygen plasma, NaOH, or piranha solution. The lysine amines can be readily modified in controllable densities using bifunctional *N*-hydroxysuccinimide (NHS) esters, allowing the attachment of a nearly limitless variety of probes.

In this work, the aMZI platform is compared to a commercially available quartz crystal microbalance with dissipation (QCM-D) in terms of the absolute response and signal-to-noise ratio. To reach this aim, biotin-modified PLL was used to reliably attach probes to both the aMZI and QCM-D chips, and the stepwise binding of increasing streptavidin concentrations to the PLL-biotin was monitored by both techniques. The final saturated binding of streptavidin and the signal-to-noise ratio were compared between the aMZI and the QCM-D.

RESULTS

The chips used for the aMZI experiments contain six parallel aMZI devices on a single chip, as can be seen in Figure 1,

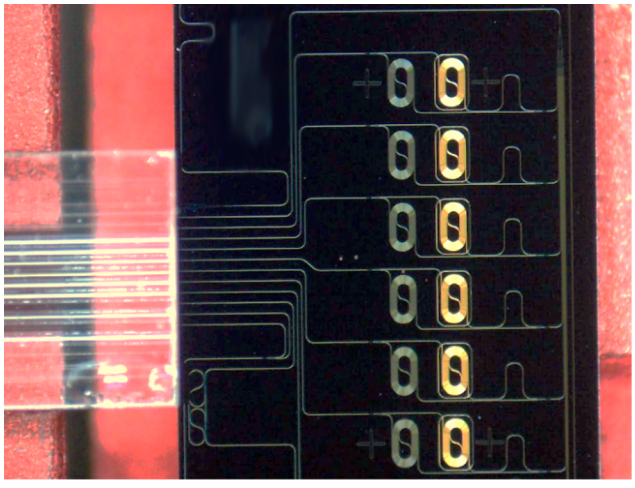

Figure 1. Photograph of an aMZI chip with lithographically defined Si_3N_4 waveguides showing the six parallel aMZI devices (arranged top to bottom). Each aMZI device consists of a reference channel (left), which is closed (covered by SiO_2), and an analyte channel (right), which is open to the flow of liquids.

allowing for six simultaneous measurements. There is a single microfluidic channel for analyte injection over the whole chip with the liquid flowing from the top to the bottom of the chip. As there are six sensing windows, six measurements can be potentially performed at the same time, pending the selective binding of probes to each sensing window in a controlled fashion.

PLL adsorbs readily to cleaned Si_3N_4, as well as the surrounding SiO_2, through electrostatic interactions and is not removed by rinsing with, or even sonicating in, buffer. Once a sample of PLL has been successfully adsorbed on the surface, the surface is saturated with PLL and no further PLL can be adsorbed, meaning that there is no run over between analytes upon washing. Adding 10% glycerol to the PLL solution helps to prevent drying of the small quantities required to cover a sensing window, which greatly eases the process when spotting by hand with a pipette. To prevent any possible crossover due to the 200 μm gaps in between the sensing windows, the top two sensors were spotted with PLL-biotin, i.e., PLL modified with the probe moiety, and the bottom two with PLL-OEG, i.e., PLL modified only with OEG chains that provide antifouling properties. A schematic of the adsorption of PLL-biotin and the subsequent binding of streptavidin and the structures of the modified PLLs can be found in Figure 2. The middle two sensors were left free to avoid any accidental mixing of the droplets and thus contamination between the two PLL analytes. The data from different spotting experiments were not always identical, and the most reliable functionalization was only obtained after submerging the full chip in the PLL solution, showing that the spotting procedure does not lead to the perfect coverage for this combination of PLL and aMZI chips. The poorer reproducibility and crossover occurring during spotting currently limit the number of different analytes that can be accurately and reproducibly measured to one, by submerging the whole chip. A reference could be added by blocking the receptors of some windows after functionalization with PLL by spotting streptavidin onto the desired reference windows to block the receptors. To increase the number of different analytes that can be measured simultaneously, further research into spotting (such as using an automated spotting device, changing the solution composition, varying the surface preparation, and cleaning methods or applying heat or mechanical agitation to help increase the PLL coverage) and/or the design of a microfluidic device (that would allow addressing the windows individually) would be required.

In contrast to the aMZI, the QCM-D consists of four separate chambers, each of which houses a chip. This makes the introduction of up to four different coatings trivial, as each chip can be processed completely separately. We chose Si_3N_4-coated QCM-D chips to best match the waveguides of the aMZI chips. On the aMZI chips, the PLL solutions were introduced by adding a drop of PLL solution in phosphate-buffered saline (PBS) with 10% glycerol to cover the whole of the sensor surface; for a direct comparison, the QCM-D chips were coated by the same method, using either PLL-OEG, as a background experiment to verify the antifouling properties of PLL-OEG, or PLL-biotin to bind the analyte streptavidin.

After the adsorption of PLL, solutions of streptavidin were put in contact with the coated substrates. The conditions of the QCM-D and aMZI experiments were chosen to be as closely relatable as possible. A flow rate of 15 μL min^{-1} was used for both techniques. For the aMZI, a syringe pump filled with PBS buffer was used to flow buffer over the chip. While the chamber was flushed with buffer, the 200 μL sample loop was filled with the streptavidin solution (0−1 μM in PBS, pH 7.2) using a separate peristaltic pump. After the loop was filled, the flow of the syringe pump over the chip was changed to include the 200 μL sample loop to allow for a smooth flow of the streptavidin solution over the chip without ever stopping the flow through the chamber housing the chip. After each addition of streptavidin, this procedure could be repeated with

https://dx.doi.org/10.1021/acsabm.0c00491
ACS Appl. Bio Mater. 2020, 3, 4566−4572

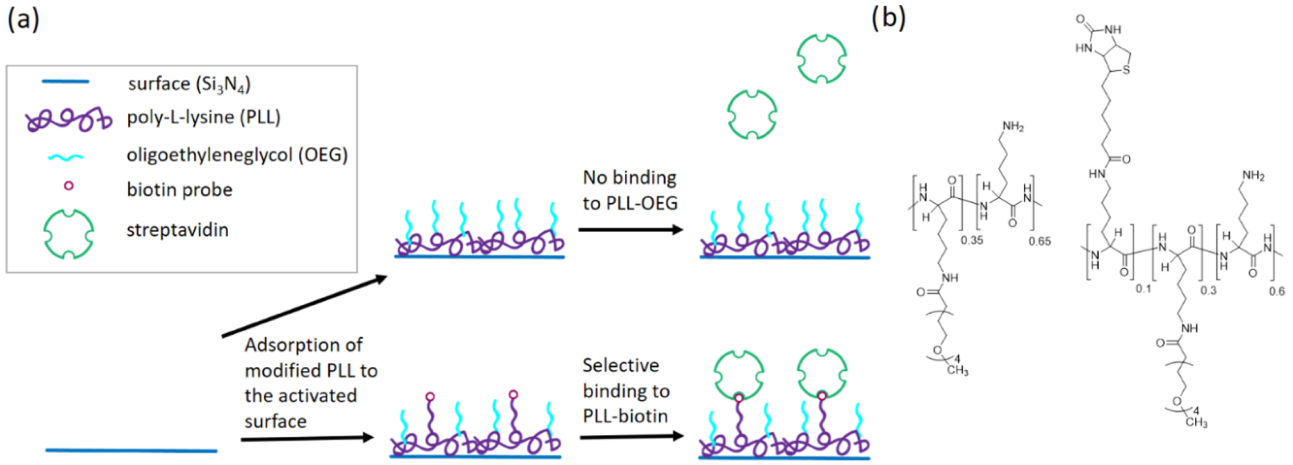

Figure 2. (a) Schematic of the adsorption of PLL-biotin and PLL-OEG, and the subsequent binding of streptavidin to the biotin moieties. (b) Structures of PLL-OEG (left) and PLL-biotin (right).

different concentrations of streptavidin. Each buffer wash step was performed for 10 min. For the QCM-D experiments, the buffer steps were performed for 10 min and the streptavidin steps for 13.3 min to achieve approximately the same volume of 200 μL, which was used in the aMZI experiments. To change the sample, the flow was stopped, the sample vials were changed, and then the flow was resumed.

In QCM experiments, a change in mass density Δm (ng cm^{-2}) on the chip is obtained by following the change in frequency Δf (Hz), and they are related to each other by the Sauerbrey equation[32]

$$\Delta m = -C\Delta f \quad (1)$$

where C is the Sauerbrey constant (17.7 Hz ng^{-1} cm^{-2}).

In these QCM-D experiments, the PLL-OEG sample shows no binding at any concentration of streptavidin as can be seen in Figure 3a. Small "waves" can be seen with the change between buffer and streptavidin and back; these arise from a change in viscosity in the solution and not from any interaction between the streptavidin and the surface. These results verify the ability of PLL-OEG as an antifouling layer for streptavidin.

The PLL-biotin-coated chip exhibits stepwise decreases in frequency upon exposure to increasing concentrations of streptavidin, which do not recover upon flushing with buffer (Figure 3b). The small peaks apparent in Figure 3b arise from the stopping and starting of the flow to change the solutions. There is a delay between the changing of the solution and the sample reaching the chamber due to the length of the tubing before the chamber. The observed frequency changes result from the binding of streptavidin to the surface, and the absence of recovery is caused by the strong, practically irreversible biotin–streptavidin interaction. Increasing the concentration of streptavidin does increase the change in frequency, as can be seen from the change between 50 and 100 nM. From concentrations of 200 nM and higher, the surfaces become saturated, and any further increase in concentration no longer changes this frequency by a significant amount. The final total change in frequency is −26 Hz, which is comparable to previous results for a complete and saturated layer of streptavidin.[33,34]

The Sauerbrey equation is only applicable when the layer formed can be assumed to be rigid. As a rule, if the change in dissipation, which is a measure of the rigidity of the layer, is

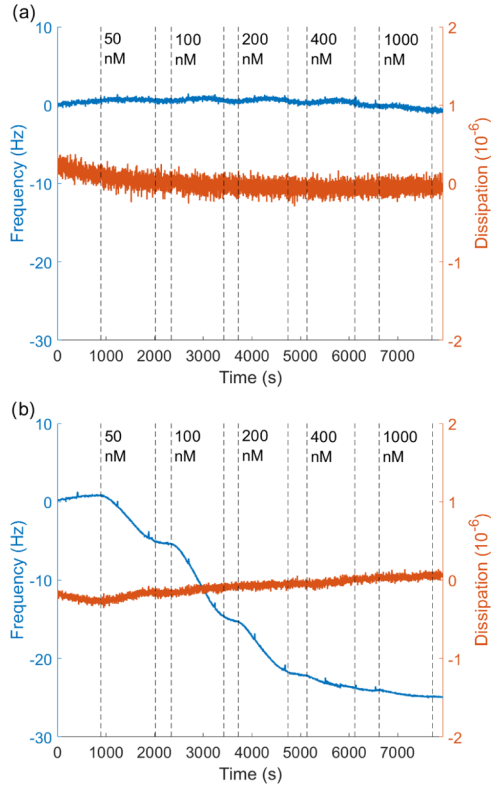

Figure 3. QCM-D (frequency, left axis, and dissipation, right axis) data of increasing concentrations of streptavidin (values given in the graph; buffer flow when no concentration is given) at substrates coated with (a) PLL-OEG and (b) PLL-biotin.

less than 2.0 × 10^{-6}, the layer can be treated as rigid.[35] The maximum dissipation change observed in the experiments was 0.35 × 10^{-6}, so it can be deemed appropriate to use the Sauerbrey equation. Using the Sauerbrey equation, a Δf of −26 Hz corresponds to a Δm of 460 ng cm^{-2}. This mass change includes all water coupled hydrodynamically to the hydrophilic streptavidin, as QCM-D measures all mass and does not differentiate between coupled water and analyte. This means that it is required to compare QCM-D results to those of other techniques if the absolute streptavidin mass density is desired.

https://dx.doi.org/10.1021/acsabm.0c00491
ACS Appl. Bio Mater. 2020, 3, 4566–4572

Figure 4 shows the data collected during the streptavidin binding experiments at the aMZI platform. When switching

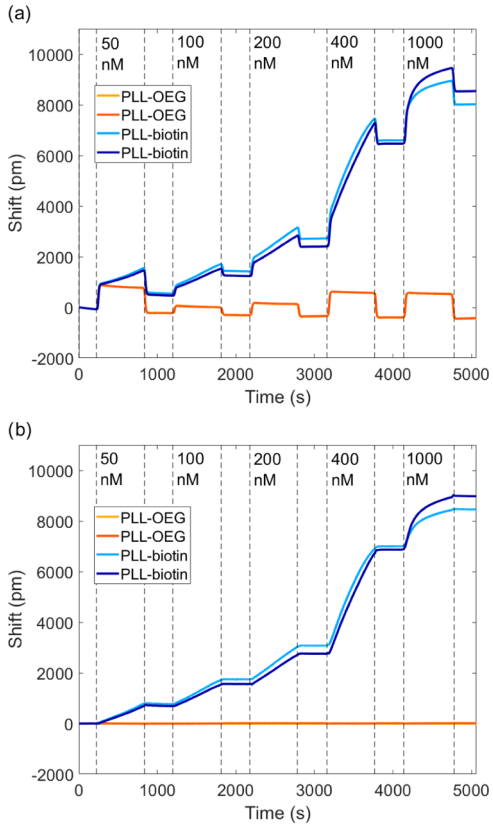

Figure 4. aMZI data showing the binding of streptavidin (values given in the graph; buffer flow when no concentration is given) to PLL-biotin: (a) raw data and (b) data with reference subtracted.

between PBS and the streptavidin solutions, there is a significant change in the refractive index, as shown in Figure 4a, recorded in the measurement as a phase shift (in pm). As the aMZI records all sensors at the same time and the PLL-OEG is an effective antifouling layer, as shown in the QCM-D experiment, it is possible to subtract this reference data in Figure 4b to subtract the effects of the bulk refractive index changes to record only the amount of binding on the surface without bulk effects.

The streptavidin binding does not saturate until the final value is reached at a concentration of 1000 nM of streptavidin. The difference between saturation concentration between QCM-D and aMZI is due to the actual flow in the chambers affecting the kinetics of binding. An in-depth analysis of adsorption kinetics and mass transport is beyond the scope of this work. Further work using higher flow rates would highlight the differences between the two techniques. Using a higher flow rate would greatly reduce the contribution of diffusion kinetics in the aMZI, allowing the fast streptavidin−biotin binding to be observed. The effects of the increased flow rate would be less significant in the QCM-D due to the large size of the sample chamber. By varying the flow rate in the aMZI, it would be possible to optimize experiments to either observe binding kinetics of strong binding events at high flow or detect low concentrations of precious analytes at a low flow rate. This flexibility would not be as easily achieved using the QCM-D. These parameters will benefit from the optimized design of the microfluidics chamber around the sensor windows, as mentioned above.

The final average shift value from the streptavidin binding experiment on the aMZI is 8722 pm ± 4%, where the variation is comparable to the typical 3% sensitivity variations found for this design right after fabrication. The slight increase is likely due to small variations in the PLL monolayer coverage and subsequent binding.

To analyze the data from the aMZI streptavidin binding and extract an adsorbed mass density, the relationship between the shift of the interference signal in pm and the protein binding should be established. Following work with comparable binding experiments on microring resonators (MRRs) with the same TriPleX technology, it was found that those MRR sensors have the same sensitivity to changes in refractive index for adsorption on the surface and for bulk changes.[22,36] Assuming the same sensitivity relationship for these aMZI devices, eq 2 (derived in the Experimental Section) can be used to calculate the mass density of streptavidin binding as

$$\Delta\Gamma = K \cdot \Delta\lambda \tag{2}$$

where $\Delta\Gamma$ is the change in mass per area in ng cm^{-2}, K is a custom-designed value of 0.029 ng pm^{-1} cm^{-2}, and $\Delta\lambda$ is the observed change in shift in pm. The average shift change of the streptavidin-saturated PLL-biotin was found to be 8722 pm, which uses eq 2 to give a mass density of 253 ng cm^{-2}.

DISCUSSION

The QCM-D and the aMZI measurements yielded mass densities of 460 and 253 ng cm^{-2}, respectively. While the QCM-D system includes hydrodynamically coupled water in the measurement, the aMZI platform does not because the adsorbed water has practically the same refractive index as the buffer and thus does not result in a measurable refractive index change. Assuming that the difference in final mass density between the two techniques can be wholly attributed to co-adsorbed water, the percentage of the water hydrodynamically coupled to the streptavidin is found to be 45% of the recorded mass in the QCM-D. Larsson et al.[33] found in their comparison between surface plasmon resonance (SPR) and QCM-D that 55% of the measured mass in the binding of streptavidin on the QCM-D was from water. This is comparable to the value achieved from our comparison of the QCM-D data with the aMZI. Both SPR and aMZI are evanescent field-based optical sensing technologies that probe the near-surface area (penetration depth ≈100−200 nm) of the liquid on top of the sensor surface for changes in the refractive index of the probe volume. Binding of protein molecules onto the sensor surface leads to such an increase in the refractive index. Both methods allow monitoring the binding of protein and to quantitatively express its adsorbed (dry) surface mass density (ng cm^{-2}). Differences could arise from the assumptions required to formulate a general equation for the technique, such as simulated sensitivities or assumptions over protein density, for both the aMZI and SPR. Another cause could be that the system measured is not exactly the same. Larsson et al. bound streptavidin to a thiol monolayer formed on gold, opposed to the PLL on Si_3N_4 used in the aMZI experiments. The addition of OEG for antifouling or the inherent hydrophilicity of the PLL backbone could make a significant difference in the environment to which the streptavidin binds when compared to thiols on gold, as well as

https://dx.doi.org/10.1021/acsabm.0c00491
ACS Appl. Bio Mater. 2020, 3, 4566−4572

the use of a different buffer, which may also affect the interactions between water and the protein.

A second metric to compare the systems is the signal-to-noise ratio. If the noise is large compared to the signal, the sensitivity and reproducibility of the technique are reduced. In Figure 3, the variance in the QCM-D frequency signal is ∼0.6 Hz. Compared with the final binding of 26 Hz, this gives a signal-to-noise ratio of 43:1. In contrast, the aMZI data in Figure 4 has a noise level of ∼1 pm and an average maximum binding of 8722 pm, giving a signal-to-noise ratio of 8722:1. Thus. the aMZI has a 200-fold improvement in the signal-to-noise ratio when compared to the QCM-D. To establish a rough estimate of the detection limit, we can extrapolate the signal given by different concentrations from the signals for both methods at the 50 nM concentration to the point where the signal would be identical to the noise level of the technique. For QCM-D, the noise limit lies at 6 nM (a signal of 5 Hz with 0.6 Hz of noise), while for the aMZI this lies at 0.07 nM (a signal of 700 pm with 1 pm of noise). This would give a 100-fold increase in the detection limit for the aMZI method for this system at these conditions. However, because of the differences in the design of the fluidics of the two systems, a true comparison of the LOD is beyond the scope of this study. Overall, this comparison shows the great potential of the aMZI as a technique to employ at low concentrations or weakly binding analytes.

CONCLUSIONS

The use of poly-L-lysine enables quick and simple attachment of bioreceptors onto both the aMZI and the QCM-D chips to allow a direct comparison between the two platforms. It was found that the aMZI measured streptavidin binding, which was comparable to literature and resulted in 45% hydrodynamically coupled water for the adsorption in the QCM-D. While the experimental conditions were chosen to best compare the two techniques, there were inevitably some differences between the systems with respect to the actual flow rates over the chip due to different chamber sizes, tubing widths, and sensor areas. For a complete study of comparable limits of detection, the binding kinetics, and mass transport, modeling of the flow within both the QCM-D and the aMZI flow chambers would be required.

Although PLL allowed the attachment of bioreceptors on both the QCM-D and aMZI chips, there was a small discrepancy in the PLL spotting consistency on the aMZI chip when doing microspotting. Even though the difference in signal is not too large to adversely affect the binding of streptavidin to biotin at the concentrations presented here, for future work, if a less strongly binding or low-concentration analyte is used, assuring a dense and complete layer of receptors would be crucial.

In conclusion, the aMZI platform proved to be a highly effective tool for biosensing compared to the established technology of QCM-D. First, it enabled the measurement of streptavidin binding without the added complication of hydrodynamically coupled water, allowing the elucidation of the absolute protein mass adsorption. Second, the aMZI exhibited a 200-fold increase in the signal-to-noise ratio and thus has the potential to have a significantly lower limit of detection. The ease of attaching up to six separate bioreceptors to the chip and measuring them all simultaneously allows the aMZI to be a flexible technique capable of self-referencing. The aMZI has the potential for label-free, low-concentration detection, and quantification of a wide variety of biological analytes.

EXPERIMENTAL SECTION

Poly-L-lysine hydrobromide (MW 15−30 kDa) was purchased from Sigma-Aldrich and dissolved in PBS (10 mM, pH 7.2) to make a stock solution of 1 mg mL^{-1}. EZ-Link (NHS-biotin) and $MS(PEG)_4$ (methyl-PEG-NHS-ester) were purchased from Thermo Fisher Scientific and dissolved in dimethyl sulfoxide (DMSO) to make a stock solution of 1 mg mL^{-1}. Streptavidin was purchased from Sigma-Aldrich and dissolved in MilliQ water to make a 1 mg mL^{-1} stock solution. All compounds were used without further purification.

PLL-biotin(10%)-OEG(30%) (PLL-biotin) and PLL-OEG(35%) (PLL-OEG) were synthesized and characterized by the methods of Duan et al.[37] The modified PLLs were dissolved in PBS (10 mM, pH 7.2) with 10% glycerol at a concentration of 1.5 mg mL^{-1}. PLL-biotin and PLL-OEG were immobilized on clean aMZI and QCM chips by dropping the solution of the desired PLL to cover the sensing windows of the aMZI and whole QCM chip. The chips were left for 5 min before being thoroughly rinsed with MilliQ water then dried under a stream of nitrogen.

QCM-D experiments were performed on a Q-Sense E4 4-channel quartz crystal microbalance with a peristaltic pump (Biolin Scientific) using a flow rate of 15 μL min^{-1} and Si_3N_4-coated quartz chips (Biolin Scientific). The equipment was equilibrated in PBS for 30 min and reagents were flushed for 13.3 min. Si_3N_4 QCM-D chips were cleaned in UV−ozone using Bioforce UV/Ozone ProCleaner Plus for 30 min.

The aMZI experiments were performed at Lionix International using a home-built setup (Figure 5). The aMZI chips were cleaned

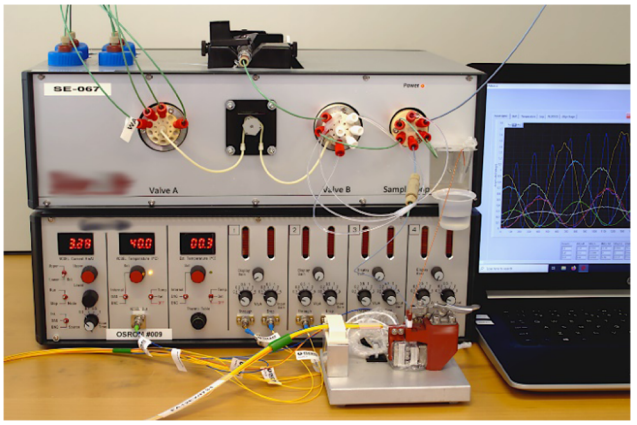

Figure 5. Photograph of the aMZI setup with the fluidic system and the piezoelectric auto-alignment stage.

using a cotton swab and a solution of 0.25 M NaOH with 1% Triton X-100, followed by thorough rinsing with deionized water and drying under a stream of nitrogen. The chips were placed in a flow cell with a piezoelectric alignment stage for the laser inputs. Experiments were performed using a 15 μL min^{-1} flow rate, a syringe pump to flush PBS (10 mM, pH 7.2), and a 200 μL sample loop with a peristaltic pump to fill the sample loop while the syringe pump never stopped the flow to the chip.

To compensate for the change in bulk refractive index (Figure 4a), the PLL-OEG data was subtracted from all sensors to give Figure 4b. To compensate for the delay due to the direction of flow over the chip (Figure 1), the data of the later sensors was shifted in time by approximately an extra 0.5 s for each subsequent sensor before subtraction.

For the analysis of the aMZI data, eq 2 was derived from a comparison to previous work on the MRR. The observed change in shift is proportional to the adsorbed mass in both MMR and aMZI. The ratio between the bulk sensitivity for aMZI and MRR is equal to the ratio in surface sensitivity giving

https://dx.doi.org/10.1021/acsabm.0c00491
ACS Appl. Bio Mater. 2020, 3, 4566−4572

$$\frac{s_{MRR}}{s_{aMZI}} = \frac{d\lambda MRR}{d\Gamma} / \frac{d\lambda aMZI}{d\Gamma} \quad (3)$$

Rearrangement of (eq 3) gives

$$\frac{d\lambda aMZI}{d\Gamma} = \frac{d\lambda MRR}{d\Gamma} \times \frac{s_{aMZI}}{s_{MRR}} \quad (4)$$

The bulk sensitivity of the MMR was calculated by Heideman et al.[22] to be

$$s_{MRR} = 98 \text{ nm RIU}^{-1}$$

The surface sensitivity, if it is assumed that proteins have an average mass density of 1.35 g cm^3, was calculated by Besselink et al.[36] to be

$$\frac{d\lambda MRR}{d\Gamma} = 1.7 \text{ pm ng}^{-1} \text{ cm}^2$$

Substitution of these values into (eq 4) and given that the sensitivity of the MZI chips is designed to be 2000 nm RIU^{-1} gives

$$\frac{d\lambda aMZI}{d\Gamma} = 1.7 \text{ pm ng}^{-1} \text{ cm}^2 \times \frac{s_{aMZI}}{98 \text{ nm RIU}^{-1}} \quad (5)$$

Rearranging and simplifying (eq 5) gives eq 2.

AUTHOR INFORMATION

Corresponding Author

Jurriaan Huskens − *MESA+ Institute for Nanotechnology, Faculty of Science and Technology, University of Twente, 7522 NH Enschede, The Netherlands;* orcid.org/0000-0002-4596-9179; Email: j.huskens@utwente.nl

Authors

Melissa J. Goodwin − *MESA+ Institute for Nanotechnology, Faculty of Science and Technology, University of Twente, 7522 NH Enschede, The Netherlands*

Geert A. J. Besselink − *Lionix International, 7500 AL Enschede, The Netherlands*

Floris Falke − *Lionix International, 7500 AL Enschede, The Netherlands*

Arnoud S. Everhardt − *Lionix International, 7500 AL Enschede, The Netherlands*

Jeroen J. L. M. Cornelissen − *MESA+ Institute for Nanotechnology, Faculty of Science and Technology, University of Twente, 7522 NH Enschede, The Netherlands;* orcid.org/0000-0002-9728-5043

Complete contact information is available at: https://pubs.acs.org/10.1021/acsabm.0c00491

Author Contributions

M.J.G. and G.A.J.B. performed the experiments and analyzed the results. All authors contributed to the writing of the manuscript.

Funding

This work was funded by OP Oost and the European Union as part of the Biomeander project.

Notes

The authors declare no competing financial interest.

ACKNOWLEDGMENTS

Dr. Almudena Marti Morant is thanked for providing the PLL-biotin.

ABBREVIATIONS

aMZI, asymmetric Mach−Zehnder interferometer; OEG, oligo(ethylene glycol); PBS, phosphate-buffered saline; PLL, poly-L-lysine; MRR, microring resonator; QCM-D, quartz crystal microbalance with dissipation; SPR, surface plasmon resonance

REFERENCES

(1) Metkar, S. K.; Girigoswami, K. Diagnostic Biosensors in Medicine − A Review. *Biocatal. Agric. Biotechnol.* **2019**, *17*, 271−283.

(2) Sireesha, M.; Jagadeesh Babu, V.; Kranthi Kiran, A. S.; Ramakrishna, S. A Review on Carbon Nanotubes in Biosensor Devices and Their Applications in Medicine. *Nanocomposites* **2018**, *4*, 36−57.

(3) Neethirajan, S.; Ragavan, V.; Weng, X.; Chand, R. Biosensors for Sustainable Food Engineering: Challenges and Perspectives. *Biosensors* **2018**, *8*, No. 23.

(4) Yoo, E. H.; Lee, S. Y. Glucose Biosensors: An Overview of Use in Clinical Practice. *Sensors* **2010**, *10*, 4558−4576.

(5) Khanmohammadi, A.; Aghaie, A.; Vahedi, E.; Qazvini, A.; Ghanei, M.; Afkhami, A.; Hajian, A.; Bagheri, H. Electrochemical Biosensors for the Detection of Lung Cancer Biomarkers: A Review. *Talanta* **2020**, *206*, No. 120251.

(6) Qian, L.; Li, Q.; Baryeh, K.; Qiu, W.; Li, K.; Zhang, J.; Yu, Q.; Xu, D.; Liu, W.; Brand, R. E.; et al. Biosensors for Early Diagnosis of Pancreatic Cancer: A Review. *Transl. Res.* **2019**, *213*, 67−89.

(7) Sanati, A.; Jalali, M.; Raeissi, K.; Karimzadeh, F.; Kharaziha, M.; Mahshid, S. S.; Mahshid, S. A Review on Recent Advancements in Electrochemical Biosensing Using Carbonaceous Nanomaterials. *Microchim. Acta* **2019**, *186*, No. 773.

(8) Blair, E. O.; Corrigan, D. K. A Review of Microfabricated Electrochemical Biosensors for DNA Detection. *Biosens. Bioelectron.* **2019**, *134*, 57−67.

(9) Batool, R.; Rhouati, A.; Nawaz, M. H.; Hayat, A.; Marty, J. L. A Review of the Construction of Nano-Hybrids for Electrochemical Biosensing of Glucose. *Biosensors* **2019**, *9*, No. 46.

(10) Wang, W.; Su, H.; Wu, Y.; Zhou, T.; Li, T. Review-Biosensing and Biomedical Applications of Graphene: A Review of Current Progress and Future Prospect. *J. Electrochem. Soc.* **2019**, *166*, B505−B520.

(11) Syu, Y. C.; Hsu, W. E.; Lin, C. T. Review-Field-Effect Transistor Biosensing: Devices and Clinical Applications. *ECS J. Solid State Sci. Technol.* **2018**, *7*, Q3196−Q3207.

(12) Garzón, V.; Pinacho, D. G.; Bustos, R. H.; Garzón, G.; Bustamante, S. Optical Biosensors for Therapeutic Drug Monitoring. *Biosensors* **2019**, *9*, No. 132.

(13) Mejía-Salazar, J. R.; Oliveira, O. N. Plasmonic Biosensing. *Chem. Rev.* **2018**, *118*, 10617−10625.

(14) Peltomaa, R.; Glahn-Martínez, B.; Benito-Peña, E.; Moreno-Bondi, M. C. Optical Biosensors for Label-Free Detection of Small Molecules. *Sensors* **2018**, *18*, No. 4126.

(15) Juan-Colás, J.; Johnson, S.; Krauss, T. F. Dual-Mode Electro-Optical Techniques for Biosensing Applications: A Review. *Sensors* **2017**, *17*, No. 2047.

(16) Bhalla, N.; Jolly, P.; Formisano, N.; Estrela, P. Introduction to Biosensors. *Essays Biochem.* **2016**, *60*, 1−8.

(17) Grieshaber, D.; MacKenzie, R.; Vörös, J.; Reimhult, E. Electrochemical Biosensors - Sensor Principles and Architectures. *Sensors* **2008**, *8*, 1400−1458.

(18) Kozma, P.; Kehl, F.; Ehrentreich-förster, E.; Stamm, C.; Bier, F. F. Integrated Planar Optical Waveguide Interferometer Biosensors: A Comparative Review. *Biosens. Bioelectron.* **2014**, *58*, 287−307.

(19) Estevez, M. C.; Alvarez, M.; Lechuga, L. M. Integrated Optical Devices for Lab-on-a-Chip Biosensing Applications. *Laser Photonics Rev.* **2012**, *6*, 463−487.

(20) Chalyan, T.; Guider, R.; Pasquardini, L.; Zanetti, M.; Falke, F.; Schreuder, E.; Heideman, R. G.; Pederzolli, C.; Pavesi, L. Asymmetric

https://dx.doi.org/10.1021/acsabm.0c00491
ACS Appl. Bio Mater. 2020, 3, 4566−4572

Mach-Zehnder Interferometer Based Biosensors for Aflatoxin M1 Detection. *Biosensors* **2016**, *6*, 1−10.
(21) Fernández-Gavela, A.; Herranz, S.; Chocarro, B.; Falke, F.; Schreuder, E.; Leeuwis, H.; Heideman, R. G.; Lechuga, L. M. Full Integration of Photonic Nanoimmunosensors in Portable Platforms for On-Line Monitoring of Ocean Pollutants. *Sens. Actuators, B* **2019**, *297*, No. 126758.
(22) Heideman, R.; Hoekman, M.; Schreuder, E. TriPleX-Based Integrated Optical Ring Resonators for Lab-on-a-Chip and Environmental Detection. *J. Sel. Top. Quantum Electron.* **2012**, *18*, 1583−1596.
(23) Gavela, A. F.; García, D. G.; Ramirez, J. C.; Lechuga, L. M. Last Advances in Silicon-Based Optical Biosensors. *Sensors* **2016**, *16*, No. 285.
(24) Bastos, A. R.; Vicente, C. M. S.; Oliveira-Silva, R.; Silva, N. J. O.; Tacão, M.; da Costa, J. P.; Lima, M.; André, P. S.; Ferreira, R. A. S. Integrated Optical Mach-Zehnder Interferometer Based on Organic-Inorganic Hybrids for Photonics-on-a-Chip Biosensing Applications. *Sensors* **2018**, *18*, No. 840.
(25) Liu, Q.; Tu, X.; Woo, K.; Sheng, J.; Shin, Y.; Han, K.; Yoon, Y.; Lo, G.; Kyoung, M. Highly Sensitive Mach−Zehnder Interferometer Biosensor Based on Silicon Nitride Slot Waveguide. *Sens. Actuators, B* **2013**, *188*, 681−688.
(26) Psarouli, A.; Botsialas, A.; Salapatas, A.; Stefanitsis, G.; Nikita, D.; Jobst, G.; Chaniotakis, N.; Goustouridis, D.; Makarona, E.; Petrou, P. S.; et al. Fast Label-Free Detection of C-Reactive Protein Using Broad-Band Mach-Zehnder Interferometers Integrated on Silicon Chips. *Talanta* **2017**, *165*, 458−465.
(27) Gauglitz, G.; Ingenhoff, J. Design of New Integrated Optical Substrates for Immuno-Analytical Applications. *Fresenius' J. Anal. Chem.* **1994**, *349*, 355−359.
(28) Brosinger, F.; Freimuth, H.; Lacher, M.; Ehrfeld, W.; Gedig, E.; Katerkamp, A.; Spener, F.; Cammann, K. A Label-Free Affinity Sensor with Compensation of Unspecific Protein Interaction by a Highly Sensitive Integrated Optical Mach-Zehnder Interferometer on Silicon. *Sens. Actuators, B* **1997**, *44*, 350−355.
(29) Song, B.; Zhang, H.; Liu, B.; Lin, W.; Wu, J. Label-Free in-Situ Real-Time DNA Hybridization Kinetics Detection Employing Microfiber-Assisted Mach-Zehnder Interferometer. *Biosens. Bioelectron.* **2016**, *81*, 151−158.
(30) Movilli, J.; Rozzi, A.; Ricciardi, R.; Corradini, R.; Huskens, J. Control of Probe Density at DNA Biosensor Surfaces Using Poly-L-Lysine with Appended Reactive Groups. *Bioconjugate Chem.* **2018**, *29*, 4110−4118.
(31) Di Iorio, D.; Marti, A.; Koeman, S.; Huskens, J. Clickable Poly-L-Lysine for the Formation of Biorecognition Surfaces. *RSC Adv.* **2019**, *9*, 35608−35613.
(32) Sauerbrey, G. Verwendung von Schwingquarzen Zur Wägung Dünner Schichten Und Zur Mikrowägung. *Z. Phys.* **1959**, *155*, 206−222.
(33) Larsson, C.; Rodahl, M.; Höök, F. Characterization of DNA Immobilization and Subsequent Hybridization on a 2D Arrangement of Streptavidin on a Biotin-Modified Lipid Bilayer Supported on SiO_2. *Anal. Chem.* **2003**, *75*, 5080−5087.
(34) Seifert, M.; Rinke, M. T.; Galla, H. J. Characterization of Streptavidin Binding to Biotinylated, Binary Self-Assembled Thiol Monolayers - Influence of Component Ratio and Solvent. *Langmuir* **2010**, *26*, 6386−6393.
(35) Vogt, B. D.; Soles, C. L.; Lee, H. J.; Lin, E. K.; Wu, W. L. Moisture Absorption and Absorption Kinetics in Polyelectrolyte Films: Influence of Film Thickness. *Langmuir* **2004**, *20*, 1453−1458.
(36) Besselink, G. A. J.; Heideman, R. G.; Schreuder, E.; Wevers, L. S.; Falke, F.; van den Vlekkert, H. H. Performance of Arrayed Microring Resonator Sensors with the TriPleX Platform. *J. Biosens. Bioelectron.* **2016**, *7*, No. 1000209.
(37) Duan, X.; Mu, L.; Sawtelle, S. D.; Rajan, N. K.; Han, Z.; Wang, Y.; Qu, H.; Reed, M. A. Functionalized Polyelectrolytes Assembling on Nano-BioFETs for Biosensing Applications. *Adv. Funct. Mater.* **2015**, *25*, 2279−2286.

https://dx.doi.org/10.1021/acsabm.0c00491
ACS Appl. Bio Mater. 2020, 3, 4566−4572